

Analysis of the Microphysical Structure of Heavy Fog Using a Droplet Spectrometer: A Case Study

NIU Shengjie^{*1} (牛生杰), LU Chunsong^{†1,2} (陆春松), LIU Yangang² (刘延刚),
ZHAO Lijuan¹ (赵丽娟), LÜ Jingjing¹ (吕晶晶), and YANG Jun¹ (杨军)

¹*Key Laboratory of Meteorological Disaster of Ministry of Education, School of Atmospheric Physics,
Nanjing University of Information Science & Technology, Nanjing 210044*

²*Brookhaven National Laboratory, Atmospheric Sciences Division, Upton, NY 11973, USA*

(Received 10 July 2009; revised 23 December 2009)

ABSTRACT

The microphysical properties of a long-lasting heavy fog event are examined based on the results from a comprehensive field campaign conducted during the winter of 2006 at Pancheng (32.2°N , 118.7°E), Jiangsu Province, China. It is demonstrated that the key microphysical properties (liquid water content, fog droplet concentration, mean radius and standard deviation) exhibited positive correlations with one another in general, and that the 5-min-average maximum value of fog liquid water content was sometimes greater than 0.5 g m^{-3} . Further analysis shows that the unique combination of positive correlations likely arose from the simultaneous supply of moist air and fog condensation nuclei associated with the advection of warm air, which further led to high liquid water content. High values of liquid water content and droplet concentration conspired to cause low visibility ($<50 \text{ m}$) for a prolonged period of about 40 h. Examination of the microphysical relationships conditioned by the corresponding autoconversion threshold functions shows that the collision-coalescence process was sometimes likely to occur, weakening the positive correlations induced by droplet activation and condensational growth. Statistical analysis shows that the observed droplet size distribution can be described well by the Gamma distribution.

Key words: fog microphysics, positive correlation, high liquid water content, low visibility, warm and moist air

Citation: Niu, S., C. Lu, Y. Liu, L. Zhao, J. Lü, and J. Yang, 2010: Analysis of the microphysical structure of heavy fog using a droplet spectrometer: A case study. *Adv. Atmos. Sci.*, **27**(6), 1259–1275, doi: 10.1007/s00376-010-8192-6.

1. Introduction

Fog is a major natural hazard in many areas of the world, including China (Guo and Zheng, 2009; Niu et al., 2010). Studies have shown that the total economic losses associated with fog impacts on air, marine, and land transportation can be comparable to those resulting from tornadoes, or, in some cases, winter storms and hurricanes (Gultepe et al., 2007). One of the most imperative factors is the low visibility induced by fog occurrence, and great efforts have been devoted to developing fog models and parameterization of fog visibility in terms of fog microphysical properties. Early studies found that fog visibility

is closely related to fog liquid water content (L) (El-drige, 1966, 1971; Tomasi and Tampieri, 1976; Pinnick et al., 1978; Kunkel, 1984). Recently, Gultepe and Milbrandt (2007) further introduced droplet concentration (N) into the parameterization of visibility to account for the effect of varying N on visibility (Gultepe et al., 2001; Gultepe and Isaac, 2004).

Observational studies have been instrumental in our understanding of fog microphysics over the last few decades (Roach et al., 1976; Pinnick et al., 1978; Hudson, 1980; Gerber, 1981, 1991; Wendisch et al., 1998; Lu et al., 2008; Gultepe et al., 2009). Such studies have shown that fog layers are heterogeneous in nature (García-García et al., 2002) and exhibit dramatic vari-

^{*} Corresponding author: NIU Shengjie, niusj@nuist.edu.cn

[†] Current address: Brookhaven National Laboratory, Atmospheric Sciences Division, Upton, NY 11973, USA.

ations in microphysical properties, with N changing up to two orders of magnitude (Gerber, 1981, 1991), and L from near-zero to 0.5 g m^{-3} (Fuzzi et al., 1992). Li (2001) summarized earlier observations in China and concluded that on average, N is increasingly higher for fogs occurring in coastal areas, to those occurring in mountainous regions, and to those in city environments, while the behavior of the mean fog droplet radius is just the opposite. This fog phenomenon appears to agree with observations in warm clouds, where an increase in aerosol concentration leads to an increase in cloud droplet concentration but a decrease in mean droplet size (Twomey, 1977).

In spite of this considerable progress, the factors that affect fog microphysics are neither fully understood nor properly parameterized in fog models, hindering fog forecasting/nowcasting (Croft et al., 1997; Gultepe et al., 2007). More observational studies with state-of-the-art instruments are needed. This is especially true in China, where past observations of microphysical characteristics were largely based on gelatin-slide impactor systems. The temporal resolution of such systems is low, and less fog samples can be collected as a result, prohibiting detailed investigation of fog microphysical characteristics.

Fog events occur rather frequently in the Nanjing area of Jiangsu Province, China (Pu and Shen, 2001). To enhance the understanding of fog properties in this region, a comprehensive field campaign was carried out at Pancheng (32.2°N , 118.7°E), Jiangsu Province, during the winter of 2006. Fog droplet size distributions were measured at a sampling frequency of 1 Hz with a FM-100 droplet spectrometer [Droplet Measurement Technologies (DMT), Boulder, Colorado, USA]. This type of spectrometer has been used and tested in many places worldwide (e.g. Eugster et al., 2006; Klemm and Wrzesinsky, 2007; Gultepe et al., 2009); however, this deployment was the first in China.

During the campaign, an exceptional deep fog event occurred from 24–27 December 2006, with visibility lower than 50 m (sometimes only several meters) lasting for around 40 h. This heavy fog caused tremendous losses. For example, eight automobiles piled up on a freeway in the northern area of Jiangsu Province, causing seven fatalities and five injuries; two ships collided in the Yangtze River, one of which sank; the Nanjing Lukou International Airport was closed; and the number of patients suffering from respiratory diseases increased considerably in hospitals.

This paper examines this disastrous fog event, with an emphasis on the variability and mutual relationships of key microphysical properties [L , N , mean radius (\bar{r}), and standard deviation (σ)]. The rest of the paper is organized as follows. Section 2 introduces the

experiment site, instruments used for data collection, and the major approaches used to calculate key properties. Section 3 presents and discusses the results, including general characteristics of microphysics, fog droplet size distribution, microphysical relationships, and physical mechanisms for extremely high L and low visibility. Concluding remarks are presented in section 4.

2. Experiment and method

2.1 Site description

The field campaign was conducted from 30 November to 27 December 2006, and the sampling site was located at Pancheng (32.2°N , 118.7°E ; 22 m above sea level), Jiangsu Province, China. The site has several unique characteristics: it is located to the north of the Yangtze River and surrounded by various pollution sources (e.g. petrochemical factories, iron/steel works, and a thermal power plant). Detailed description of this site is available in Lu et al. (2010).

2.2 Instruments

The measurements taken during the field campaign included fog droplet spectra, visibility, routine surface meteorological variables, and planetary boundary layer structure. As mentioned above, the size distributions of fog droplets were measured with a FM-100 droplet spectrometer (Gultepe and Milbrandt, 2007; Gultepe et al., 2009) (Fig. 1). This instrument detects the number and size of individual fog droplets based on the forward light scattering by small particles. Particles scatter light from a laser diode of approximately 50 mW, and collecting optics guide the light from 5° to 14° into forward and masked (qualifier) detectors.

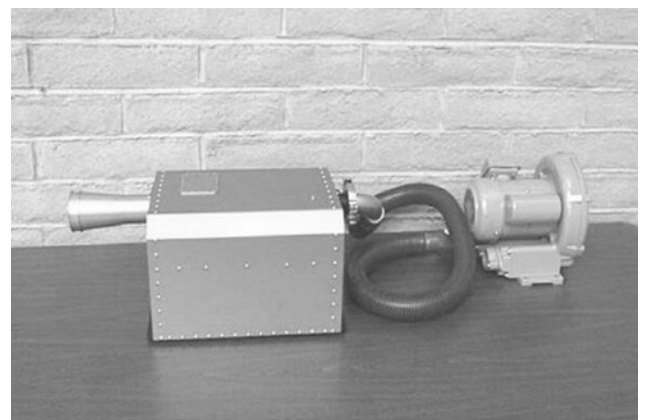


Fig. 1. The droplet spectrometer [model FM-100, Droplet Measurement Technologies (DMT), Boulder, Colorado, USA].

The vacuum source pulls fog particles through a sample area at a known velocity, allowing particle concentrations to be calculated. The intensity of the scattered light is then related to the droplet size. It measures fog droplets of 2–50 μm in diameter, and can classify droplets up to 40 size classes. The calibration of the instrument was carried out by the manufacturer using glass beads of various sizes (7.8, 15.4, 19.9, 20.6, and 40.0 μm). The difference in optical properties of the glass beads as compared to water was taken into account in the calibration process. During this experiment, the instrument was set up 1 m above the surface, and the mode with 20 size classes was selected.

Visibility was automatically measured and recorded every 15 seconds by a ZQZ-DN visibility meter, a product of the Radio Scientific Research Institute, Jiangsu Province, China. This instrument was designed according to the Guide to Meteorological Instruments and Methods of Observation (sixth edition) from the World Meteorological Organization (WMO). Both the transmitter and receiver slope downwards for 13° and outwards for 10°, and the forward scattering angle is about 33°. In order to eliminate the influence of background light on the accuracy of visibility, the measurement system was modulated with a rectangular wave. When the transmitter emits a near-infrared pulse of wavelength 930 nm with steady intensity, both the scattering energy from gas molecules, liquid and solid particles in the sampling volume and the energy of background light are collected by the receiver. When the transmitter is turned off, the receiver obtains only the energy of background light. The difference between these two pieces of received energy is the scattering energy from gas molecules and particles. With the difference value, visibility can be calculated. The relative error of the instrument is $\pm 10\%/\pm 20\%$ when the visibility is less/greater than 1000 m.

Surface meteorological quantities (surface temperature, relative humidity, wind speed, and wind direction) were observed with an automatic weather station (EnviroStation™, ICT International Pty Ltd, Armidale, New South Wales, Australia). All sensors have 16-bit resolution and an accuracy of 1%–3%.

The Vaisala DigiCORA III tethersonde system was used to probe the planetary boundary layer (PBL). The measurements of temperature, pressure, humidity, wind speed and direction at various heights were delivered and saved in the computer and their vertical profiles were automatically displayed with a vertical resolution of 1–5 m. A F-thermocap capacitive wire, H-humicap thin film capacitor, barocap silicon sensor, three-cup anemometer, and digital compass were employed to measure temperature, humidity,

pressure, wind speed, and wind direction, with resolutions 0.1°C, 0.1%, 0.1 hPa, 0.1 m s⁻¹, and 1°, respectively. In general, observations were performed every 3 h on fog-free days, and every 1–1.5 h on fog days if weather conditions (e.g. wind speed) permitted. The balloon was raised 600–1000 m high to meet the needs of fog research, and every observation lasted about 40 min.

2.3 Calculation method

According to the Fog Monitor Operator Manual provided by DMT, the true air speed (TAS, in units of m s⁻¹) of the spectrometer is calculated using the expression

$$\text{TAS} = 20.06 \times M \times T_a^{0.5}, \quad (1)$$

where M is the Mach number derived from the dynamic (pitot) pressure and static pressure (in units of millibars) (see appendix A for details), and T_a is the actual ambient temperature (in units of K). The sampling volume per second (V , in units of cm³ s⁻¹) is calculated via the following equation:

$$V = \text{TAS} \times S, \quad (2)$$

where $S = 0.264 \text{ mm}^2$ is the sampling area. The fog droplet counts divided by V provide $n(r)$ in cm⁻³ (r is the droplet radius). N (in units of cm⁻³) and L (in units of g m⁻³) of the whole spectra can be calculated, respectively, as follows:

$$N = \sum n(r), \quad (3)$$

$$L = 1 \times 10^{-6} \times \rho \times \sum \frac{4\pi}{3} r^3 n(r), \quad (4)$$

where r (in units of μm) is the geometric average radius of every size interval, and $\rho=1 \text{ g cm}^{-3}$ is the density of water. In general, the k -order radius moment (m_k) can be calculated with the following expression:

$$m_k = \sum r^k \frac{n(r)}{N} \quad (k = 0, 1, 2, \dots). \quad (5)$$

In terms of the k -order radius moment, \bar{r} and σ are given by Eqs. (6) and (7), respectively:

$$\bar{r} = m_1, \quad (6)$$

$$\sigma = (m_2 - m_1^2)^{\frac{1}{2}}. \quad (7)$$

where m_1 and m_2 are 1-order and 2-order radius moment, respectively.

3. Results and discussion

3.1 General characteristics

The fog event began at around 2208 LST (LST=UTC+8 h) 24 December 2006 and dissipated

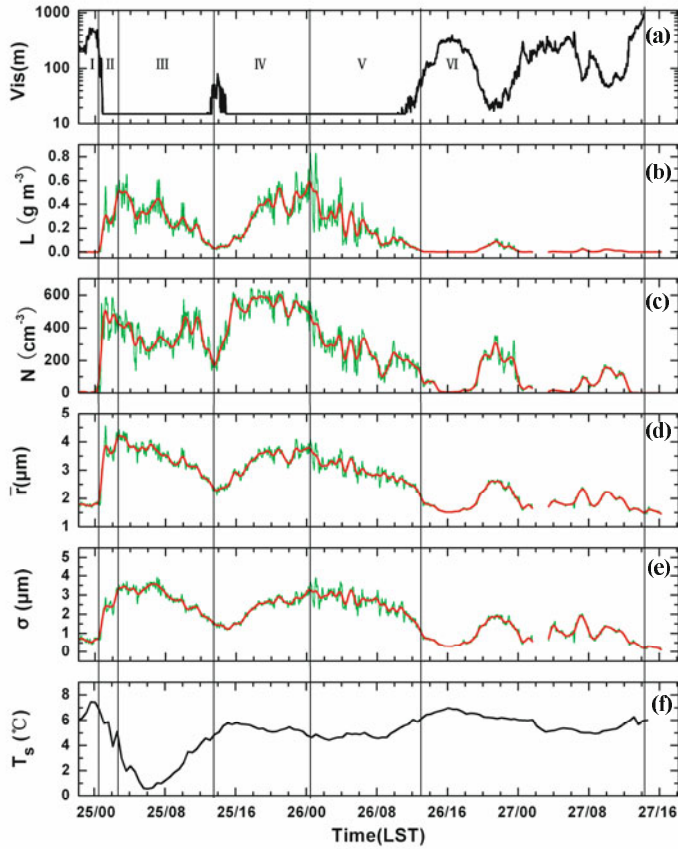


Fig. 2. The temporal variations of (a) visibility (Vis), (b) liquid water content (L), (c) number concentration (N), (d) average radius (\bar{r}), (e) standard deviation (σ), and (f) surface temperature (T_s). The green lines are 5-min-average values and the red lines are based on the results of 1800 s Fast Fourier Transform (FFT) smoothing of instantaneous values (1 Hz) in (b)–(e). During the whole period, the microphysical data between 0136 and 0327 LST 27 December 2006 were not available because of instrumental problems. I Formation stage (2208 LST 24 December to 0035 LST 25 December 2006); II Ascending period of the first L oscillation during the development stage (0035–0245 LST 25 December 2006); Descending period of the first L oscillation during the development stage (0245–1335 LST 25 December 2006); IV Ascending period of the second L oscillation during the development stage (1335 LST 25 December to 0018 LST 26 December 2006); V Descending period of the second L oscillation during the development stage (0018–1300 LST 26 December 2006); VI Dissipation stage (1300 LST 26 December to 1414 LST 27 December 2006).

at 1414 LST 27 December 2006, lasting for more than 60 h. Visibility of less than 50 m occurred between 0042 LST 25 December and 1300 LST 26 December 2006, and between 1931 and 2311 LST 26 December 2006, lasting for about 40 h (Fig. 2a). It is noteworthy that the visibility was sometimes as low as only several meters. Fog events with such a low visibility and such a long duration occur rarely in this region.

Figures 2b–2e further demonstrate the temporal variations of L , N , \bar{r} , and σ , respectively. It is clear

from these figures that throughout the fog event, the microphysical properties all exhibit two primary oscillations and two secondary ones. Similar variation holds for the temporal evolution of the fog droplet spectra (Fig. 3).

According to the variations of visibility and L , this fog event can be roughly divided into three stages: formation stage (2208 LST 24 December to 0035 LST 25 December 2006); development stage (0035 LST 25 December to 1300 LST 26 December 2006); and dissip-

Table 1. Means and standard deviations (in parenthesis) of key microphysical properties during different stages/periods and the whole fog event.

	Microphysical variables					
	Liquid water content L (g m^{-3})	Concentration N (cm^{-3})	Average radius \bar{r} (μm)	Spectra standard deviation (σ)	Maximum radius r_{\max} (μm)	Peak radius r_p (μm)
I	0.001 (0.001)	8.7 (12.8)	1.9 (0.1)	0.8 (0.1)	4.0 (0.5)	1.4 (2.5×10^{-2})
II	0.285 (0.158)	426.8 (140.2)	3.6 (0.7)	2.4 (0.7)	14.5 (3.4)	1.4 (1.8×10^{-2})
III	0.283 (0.141)	341.4 (87.3)	3.4 (0.5)	2.8 (0.6)	19.0 (1.9)	1.4 (2.0×10^{-3})
IV	0.297 (0.177)	484.4 (123.0)	3.2 (0.5)	2.3 (0.6)	18.9 (3.0)	1.4 (1.3×10^{-3})
V	0.206 (0.172)	256.1 (99.2)	3.0 (0.4)	2.6 (0.6)	19.6 (2.7)	1.4 (1.1×10^{-3})
VI	0.013 (0.022)	78.4 (83.7)	1.9 (0.3)	1.0 (0.5)	8.9 (4.5)	1.4 (1.0×10^{-3})
The whole event	0.158 (0.178)	240.1 (185.0)	2.7 (0.8)	1.9 (1.0)	14.5 (6.4)	1.4 (9.8×10^{-3})

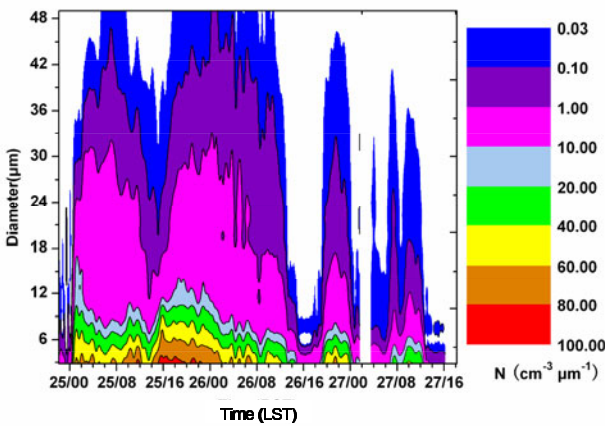


Fig. 3. The temporal evolution of spectra based on 5-min-average values.

tion stage (1300 LST 26 December to 1414 LST 27 December 2006). The development stage can further be divided into four distinct periods: ascending period of the first L oscillation (0035–0245 LST 25 December 2006); descending period of the first L oscillation (0245–1335 LST 25 December 2006); ascending period of the second L oscillation (1335 LST 25 December to 0018 LST 26 December 2006); and descending period of the second L oscillation (0018–1300 LST 26 December 2006). The major properties for each stage/period are summarized in Table 1.

It is evident that, with the exception of the peak

radius (r_p), which remains largely unchanged at 1.4 μm during the whole event, the other microphysical quantities vary substantially. Similar fog characteristics have also been reported by Huang et al. (2000). The mean N of this fog event is 240.1 cm^{-3} , only 15.8% of a 1996 fog event observed at the same site (Li, 2001). It is also lower than fog events observed in industrial cities, such as Chongqing ($29.6^\circ\text{N}, 106.5^\circ\text{E}$), China (Li et al., 1992). On the other hand, the value is comparable with that observed in Mengyang ($22.1^\circ\text{N}, 100.9^\circ\text{E}$), Yunnan Province, and Chengdu ($30.7^\circ\text{N}, 104.1^\circ\text{E}$), Sichuan Province, China (Li et al., 1992), and higher than that in Sierra Madre Oriental, Mexico (García-García et al., 2002), Waldstein, Germany (Klemm and Wrzesinsky, 2007), and Pico del Este, Puerto Rico (Eugster et al., 2006). As for L , although the average is comparable with many other events, the maximum 5-min-average exceeds 0.5 g m^{-3} (Fig. 2b), while in other studies L has usually been lower than this figure (e.g. Li, 2001; Eugster et al., 2006; Beiderwieden et al., 2007). \bar{r} , r_p , and maximum radius (r_{\max}) are similar to those observed at Pancheng in 1996 (Li, 2001).

3.2 Analytical expression for fog droplet size distribution

Over the last few decades, and owing to its broad-ranging usefulness, great effort has been devoted to finding an appropriate analytical expression for describing droplet size distribution. The Gamma function has been commonly used for this purpose (e.g.

Costa et al., 2000; Hsieh et al., 2009), such that

$$n(r) = N_0 r^\mu e^{-\lambda r}, \quad (8)$$

where r and $n(r)$ are the droplet radius and the number of droplets per unit volume per unit radius interval, respectively; and N_0 , λ , and μ are the intercept, slope, and shape parameters, respectively.

Most previous studies on analytical size distributions have been based on empirical curve-fittings to individual measured distributions. Since a droplet size distribution is the end result of many complex processes that can be considered to be stochastic in nature, such as collision and coalescence (Jaw, 1966), statistical approaches that are applicable to a large number of individual size distributions are more desirable. Liu (1992, 1993) proposed such a simple statistical method based on the relationship between the skewness and kurtosis of the raindrop size distribution to identify the statistical distribution pattern. Liu and Liu (1994) and Liu et al. (1995) further applied a similar approach to study aerosol and cloud droplet size distributions. Here, the Liu approach is applied to investigate if the statistical pattern of the fog droplet size distribution follows the Gamma distribution, and if there are any pattern differences among the different stages and periods. Briefly, skewness (S_k) and kurtosis (K_u) are defined as:

$$S_k = \frac{\int (r - \bar{r})^3 \frac{n(r)}{N} dr}{\left[\int (r - \bar{r})^2 \frac{n(r)}{N} dr \right]^{3/2}}, \quad (9a)$$

$$K_u = \frac{\int (r - \bar{r})^4 \frac{n(r)}{N} dr}{\left[\int (r - \bar{r})^2 \frac{n(r)}{N} dr \right]^2} - 3, \quad (9b)$$

In terms of the k -order radius moments, the above two equations can be rewritten:

$$S_k = \frac{m_3 - 3m_1 m_2 + 2m_1^3}{(m_2 - m_1^2)^{3/2}}, \quad (10a)$$

$$K_u = \frac{m_4 - 4m_1 m_3 + 6m_1^2 m_2 - 3m_1^4}{(m_2 - m_1^2)^2} - 3. \quad (10b)$$

For the Gamma distribution given by Eq. (7), it can be shown that

$$S_k = \frac{2}{\sqrt{1+\mu}}, \quad (11a)$$

$$K_u = \frac{6}{1+\mu}. \quad (11b)$$

Equations (11a) and (11b) indicate that $S_k = 2$ and $K_u = 6$ are for the exponential distribution with $\mu=0$.

With the classical exponential distribution as a reference, the skewness and kurtosis deviation coefficients (C_s and C_k) are introduced, such that

$$C_s = \frac{S_k^2}{4}, \quad (12a)$$

$$C_k = \frac{K_u}{6}. \quad (12b)$$

It is obvious that for the Gamma distribution, we have

$$C_s = C_k = \frac{1}{1+\mu}. \quad (13)$$

In the $C_s - C_k$ diagram, each (C_s, C_k) pair represents an individual droplet size distribution; the general Gamma distribution with varying μ satisfies the diagonally straight line.

It is evident from Fig. 4 that the values of C_s and C_k from all the 5-min-average droplet spectra fall near the straight line, suggesting that fog droplet size distributions of the whole event can be described well by the Gamma distribution. For comparison, also shown in Fig. 4 are the pairs of C_s and C_k derived from the average spectra during the whole fog event and different stages/periods displayed in Fig. 5. Obviously, these averaged droplet size distributions follow the Gamma distribution ($C_s = C_k$) as well.

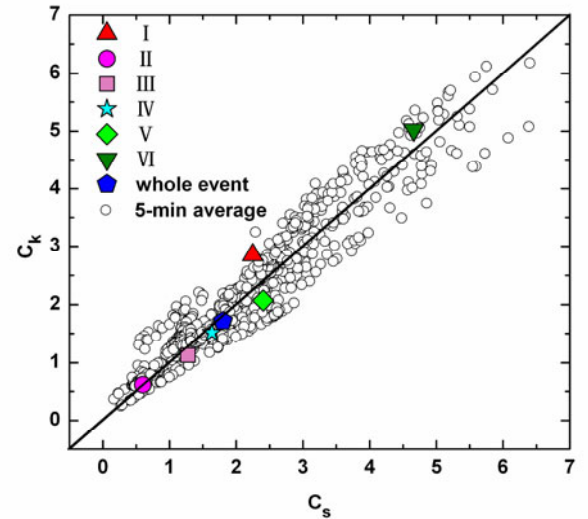


Fig. 4. Kurtosis deviation coefficients, C_k , as a function of skewness deviation coefficients, C_s . The colored symbols represent C_s and C_k of average spectra during six stages/periods (I–VI, as defined in Fig. 2) and the whole fog event; the black cycles are the 5-min-average values calculated from observations, and the solid line represents the relationship between C_s and C_k for a gamma distribution.

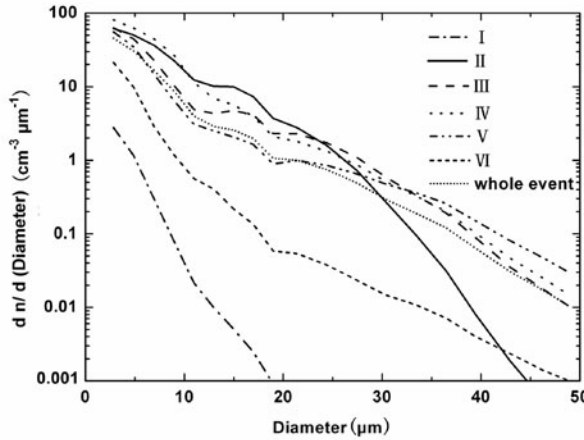


Fig. 5. Average spectra of the six stages/periods (I–VI), as defined in Fig. 2 and the whole fog event.

3.3 Microphysical relationships

To understand the physical processes responsible for this unusual fog phenomenon, this section explores the mutual relationships between the key microphysical properties. Figure 6a shows the relationship of \bar{r} to N for the whole fog event. Of note is the phenomenon that \bar{r} and N during the fog event are positively correlated with each other. This positive \bar{r} – N correlation differs from many previous studies (Li et al., 1999b;

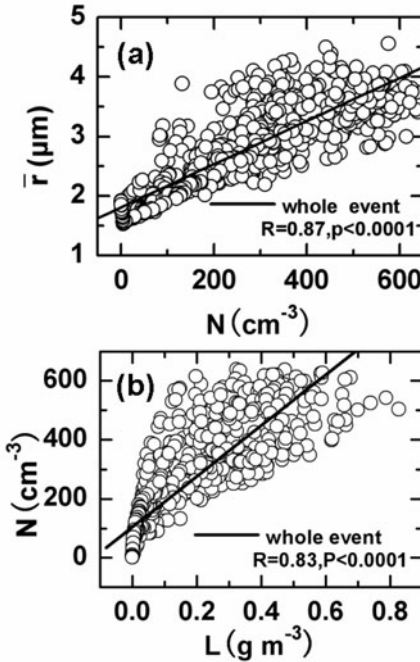


Fig. 6. (a) Average radius (\bar{r}) as a function of number concentration (N) and (b) N as a function of liquid water content (L) during the whole fog event.

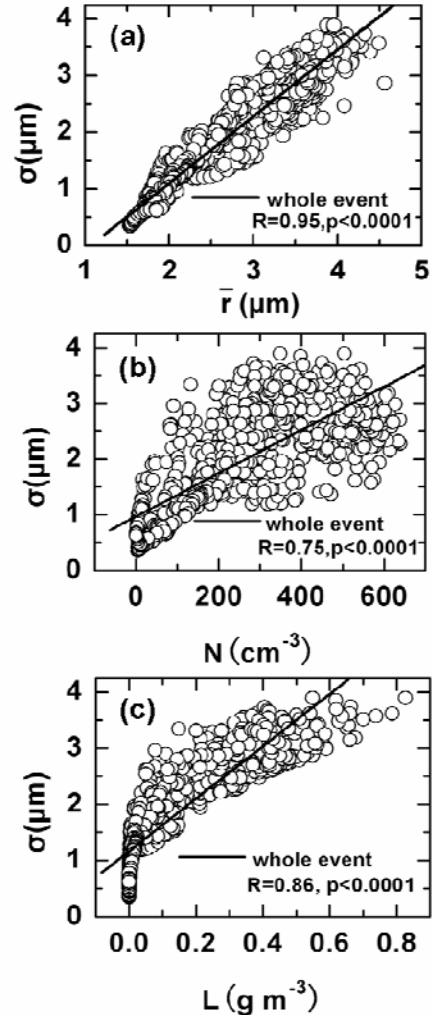


Fig. 7. (a) Standard deviation (σ) of fog spectra as a function of average radius (\bar{r}), (b) σ as a function of number concentration (N), and (c) σ as a function of liquid water content (L) during the whole fog event.

Huang et al., 2000; Tang et al., 2002), and runs against the conventional wisdom that more aerosols result in more droplets and a smaller mean radius when L remains unchanged. However, the positive \bar{r} – N correlation suggests concurrent increases of N and L , which is clearly demonstrated in Fig. 6b. Droplet activation with subsequent condensational growth (deactivation via complete droplet evaporation) can lead to co-increases (co-decreases) of N and L . The collection (collision and coalescence) process can also alter N and L simultaneously; however, it likely induces a negative, rather than positive correlation between N and L . Therefore, the positive N – L correlation is further indicative of the dominance of two contrasting processes: droplet activation with subsequent condensational growth and/or droplet deactivation via some

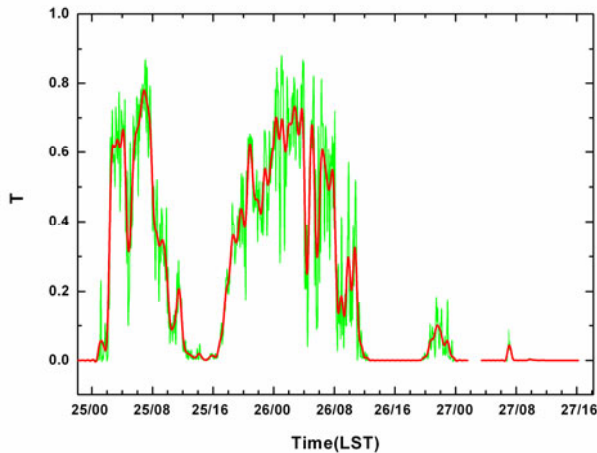


Fig. 8. Same to Fig. 2, but for the temporal variation of threshold function (T).

complete droplet evaporation.

To further dissect whether droplet deactivation via some complete droplet evaporation has a major role in determining the microphysics in this fog, the relationship of σ to \bar{r} , N , and L (Figs. 7a, b, and c) can be examined. It is clear that σ is positively correlated with \bar{r} , N , and L as well. Recognizing that droplet evaporation associated with the conventional entrainment-mixing processes (Liu et al., 2002) is unlikely to lead to the concurrent increases of σ , \bar{r} , N , and L , one can speculate that the processes of droplet deactivation and droplet evaporation in this fog, if they occur, are largely reversible to the process of droplet activation and condensational growth.

It is noteworthy that the dominance of droplet activation with subsequent condensational growth or reversible evaporation does not rule out the roles of other processes completely. For example, according to the researchers who made the measurements, drizzling sometimes occurred during this fog event (unfortunately, no direct measurements of drizzle-sized drops were made during this event), which suggests the action of the collection process. To examine the strength of the collection process in this fog event, the autoconversion threshold function (T) proposed by Liu et al. (2005, 2006) was calculated (see appendix B for details). A larger value of T indicates a stronger collection process, ranging from no action ($T = 0$) to full action ($T = 1$). The results (Fig. 8) agree favorably with the observers' report that drizzling sometimes occurred during the fog event. Moreover, during the fog event, 5-min-average values of T span a wide range, from 0 to 0.87, providing a great opportunity to examine the influence of the collection process on the microphysical relationships discussed above. For this purpose, the dataset was classified into three groups ($0 \leq T \leq 0.2$, $0.2 < T < 0.6$, and $0.6 \leq T \leq 1.0$),

and the microphysical relationships among the three groups are contrasted (Fig. 9). In general, a higher T tends to correspond to a weaker positive correlation, or even irrelevance, negative correlation between the microphysical properties. In other words, the collection process tends to destroy the positive correlation, as some big droplets grow by collecting small ones and result in increases of \bar{r} and σ , but a decrease of N .

Moreover, it is anticipated that different microphysical processes act in different stages/periods with different combinations, and that the exact microphysical relationships are determined by the degree of balance between these processes. This complex nature is evident from Figs. 10–14, which compare the microphysical relationships in different stages/periods, the results from which are discussed below.

During the formation and dissipation stages, the size distributions are relatively narrow (Fig. 3). Although there are two short-period developments in the dissipation stage, the concentrations of big droplets with radius $> 10 \mu\text{m}$ are very low (Fig. 15). Therefore, in the formation stage and the ascending periods of the secondary L oscillations in the dissipation stage, droplet activation and condensation should be dominant, leading to strong positive correlations. While in the descending periods of the secondary L oscillations, in addition to evaporation, turbulent mixing may also be a factor.

During the development stage the droplet spectra are broad, with large concentrations of big droplets (radius $> 10 \mu\text{m}$), indicating that the processes of collection are likely to be important factors (Figs. 3 and 15). If collection was the main microphysical process, \bar{r} and N would be negatively correlated with each other. However, during the second L oscillation, the correlation coefficients are positively high, which is closely related to droplet activation with subsequent condensational growth. In this period, southern winds above the temperature inversion are stronger than those at the surface and adjacent layers, indicating more remarkable warm advection above the inversion (Fig. 16). As a result, the temperature above the inversion is always higher than the surface and adjacent layer, even after sunrise, so the inversion is maintained at a stable level. At the same time, southerly moisture advection provides a substantial amount of water vapor which accumulates under the inversion.

In addition to a sufficient supply of moisture, a considerable quantity of aerosol particles discharged from nearby industrial activities accumulated. Based on Tong (2008), aerosol concentration at Pancheng is high and water soluble materials are major compositions of the aerosol particles, providing a sufficient source of fog condensation nuclei in this area. As a

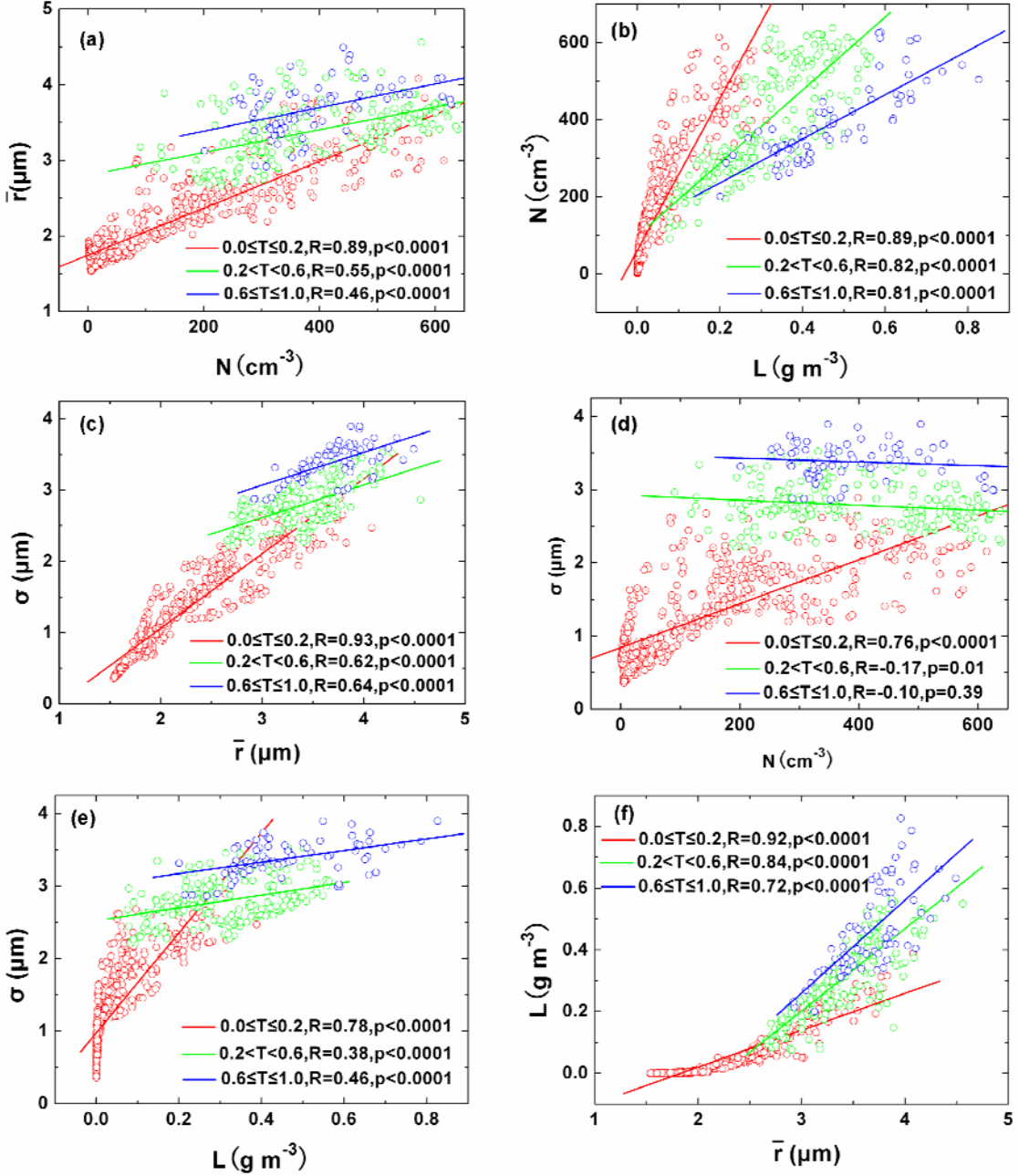


Fig. 9. (a) Average radius (\bar{r}) as a function of number concentration (N), (b) N as a function of liquid water content (L), (c) standard deviation (σ) as a function of \bar{r} , (d) σ as a function of N , (e) σ as a function of L , and (f) L as a function of \bar{r} with different T ranges.

result, the small droplets are reproduced through droplet activation, with subsequent condensational growth promoted by sufficient supplies of water vapor and fog condensation nuclei. These new small droplets may compensate for the loss caused by collection. As a result, the evolution of small droplet number concentration is almost in phase with that of big ones (Fig. 15). \bar{r} is mainly determined by big droplets, while N is

contributed to dominantly by small ones. Therefore, \bar{r} and N show a positive correlation in the second L oscillation (Fig. 10c), and the concurrent variations of σ , \bar{r} , N , and L are also expected (Figs. 11c, 12c, 13c, and 14c).

Unfortunately, in the first L oscillation, the entire set of observations of the boundary layer structure was not available. However, as can be seen from the high

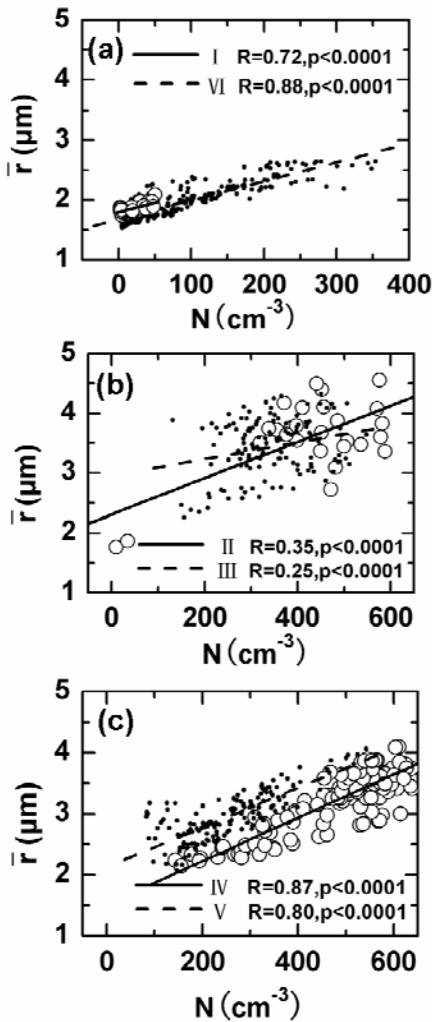


Fig. 10. Average radius (\bar{r}) as a function of number concentration (N) during the different stages/periods (I–VI), as defined in Fig. 2.

wind speed center above 200 m after 0700 LST 25 December 2006 (Fig. 16a), it is believed that the warm and moist air exists in the whole first L oscillation. Different from the second L oscillation, the correlation coefficients of \bar{r} vs. N are relatively lower, but still positive (Fig. 10b). In the ascending period of the first L oscillation, temperature decreases due to longwave radiation (Fig. 2f), causing the development of activation and condensation. As a result, small droplets increase remarkably at 0110 LST 25 December 2006 (Fig. 15). Then, the broadening of spectra is very sudden from 0110 LST to 0245 LST 25 December 2006, with a rapid increase of big droplets, indicating that the collection develops and consumes small droplets. As a result, small droplets decrease sharply during this time, and the positive correlation of \bar{r} and N in this period is not very significant. Similarly, the correlation coefficients of N vs. L and σ vs. N are lower (Figs. 11b

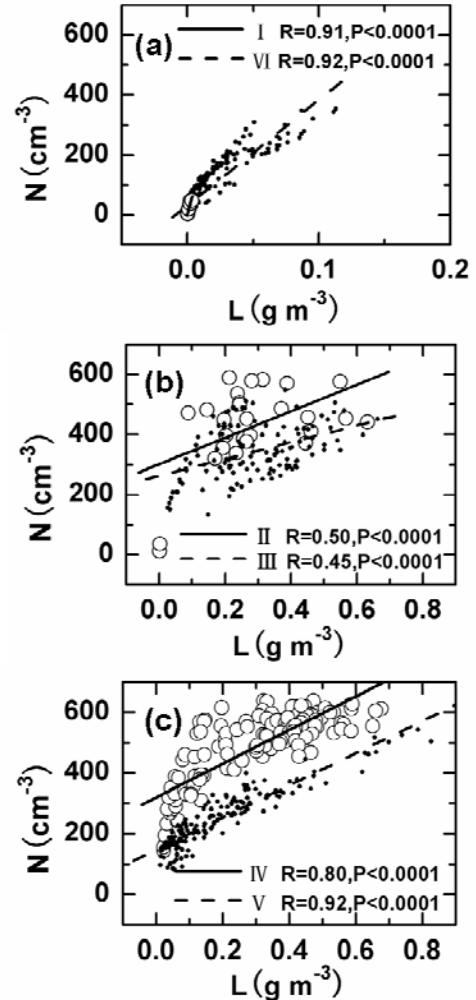


Fig. 11. Number concentration (N) as a function of liquid water content (L) during the different stages/periods (I–VI), as defined in Fig. 2.

and 13b), but σ still has a good positive correlation with \bar{r} and L (Figs. 12b and 14b).

During the descending period of the first L oscillation, human activities after sunrise (0655 LST 25 December 2006) provide plenty of fog condensation nuclei, producing a large number of small droplets through droplet activation and condensation. As a result, during the period 0842–1240 LST 25 December 2006, two obvious peaks of small droplet concentration are achieved (Fig. 15). However, the peaks of big droplet concentration are weak, resulting in only small variation of \bar{r} (Fig. 2d). Then, positive correlation between N and \bar{r} is not that significant during the whole period (Fig. 10b). Due to the very high positive correlation coefficient of σ and \bar{r} (Fig. 12b), the variation of σ is expected to be similar to \bar{r} , with small variation during the period 0842–1240 LST 25 December 2006. This might be the main reason for

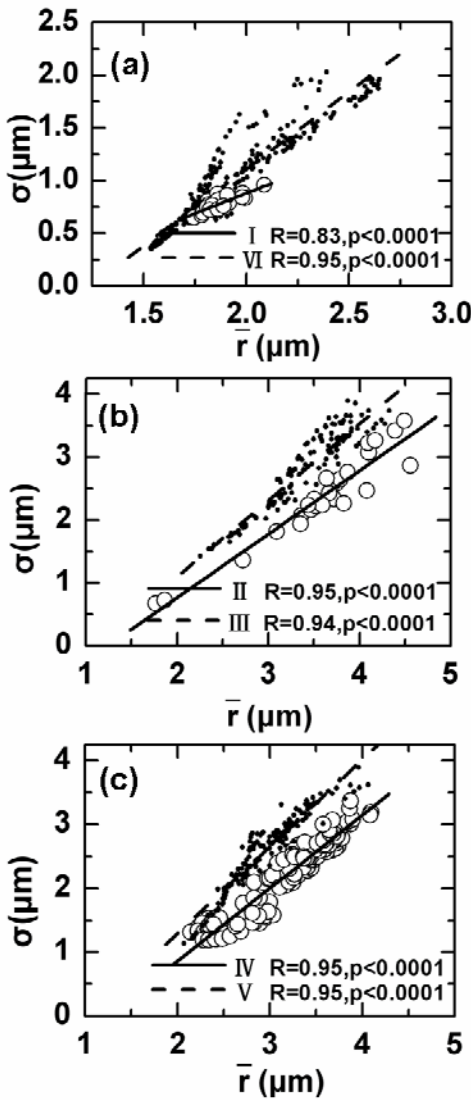


Fig. 12. Standard deviation (σ) of fog spectra as a function of average radius (\bar{r}) during the different stages/periods (I–VI), as defined in Fig. 2.

the poor correlation between σ and N (Fig. 13b) during this period.

In general, with the development of collection during the development stage, small droplets (radius $\leq 10 \mu\text{m}$) with $0.2 < T < 0.6$ are almost equal to those with $0.6 \leq T \leq 1.0$ (Fig. 17), suggesting that although the formation of big droplets (radius $> 10 \mu\text{m}$) consumes small ones, the production of small ones through activation with subsequent condensational growth can compensate for the loss caused by collection, which provides further evidence to support the conclusion that droplet activation with subsequent condensational growth is the predominant process.

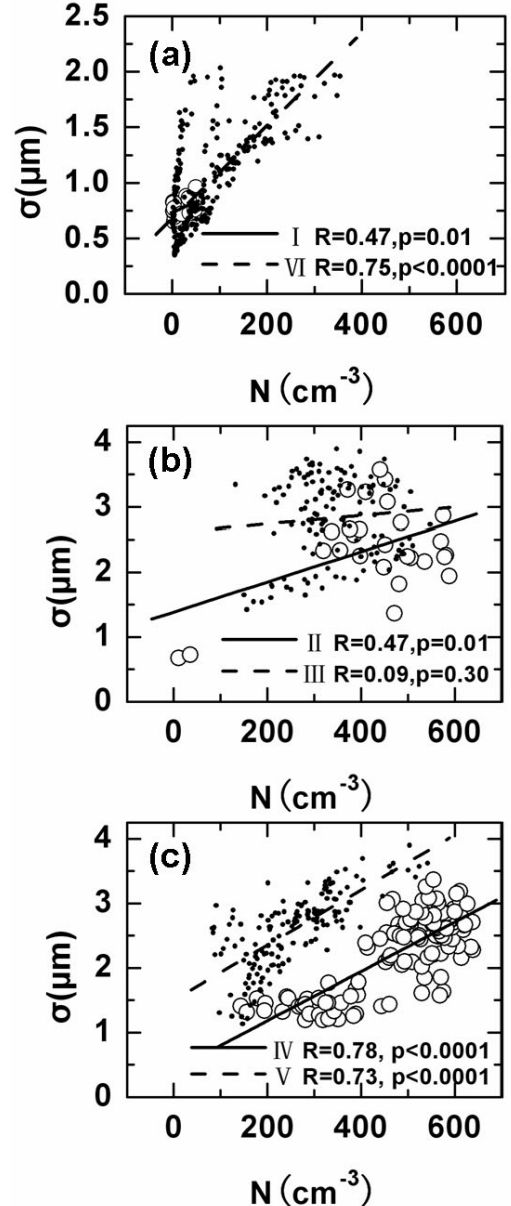


Fig. 13. Standard deviation (σ) of fog spectra as a function of number concentration (N) during the different stages/periods (I–VI), as defined in Fig. 2.

3.4 Physical reasons for high liquid water content and low visibility

Another striking feature of this fog event is its high maximum L and low visibility. As shown in Fig. 2b, during the two nights of the development stage, L reaches its 5-min-average maximum of $> 0.5 \text{ g m}^{-3}$. Furthermore, as mentioned above, visibility of $< 50 \text{ m}$ lasts for around 40 h, with sometimes only several meters of visibility (Fig. 2a). This section explores the physical reasons for the unusually high L and low visi-

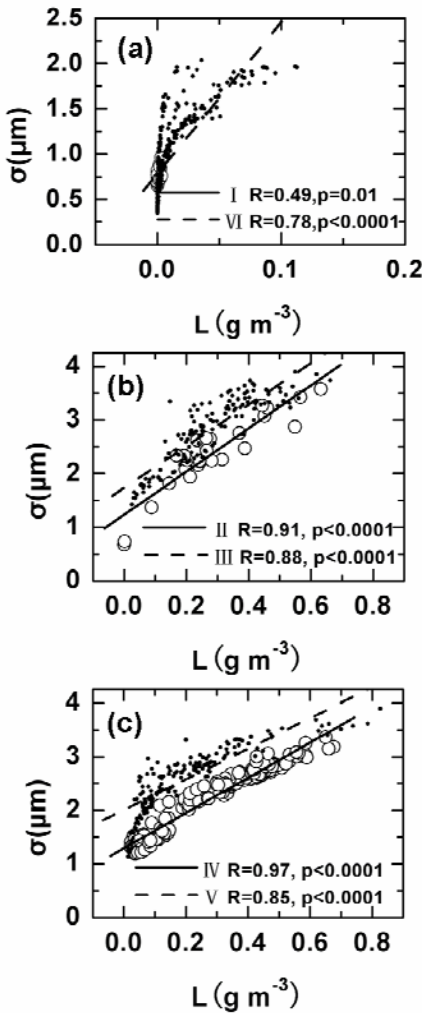


Fig. 14. Standard deviation (σ) of fog spectra as a function of liquid water content (L) during the different stages/periods (I–VI), as defined in Fig. 2.

bility.

As shown above, in general the key quantities of N , L , σ , and \bar{r} are positively correlated to one another during the whole event. The synchronous increase of N , σ , \bar{r} and L is the first microphysical reason for high L . Another reason is closely related to the high fog top (200–600 m) (Fig. 16c), which is higher than many fog events previously reported (Pilié et al., 1975; Roach et al., 1976; Guedalia and Bergot, 1994; Li et al., 1999a, b). Other things being equal, a higher top allows more time for droplets to grow larger, leading to a higher L , as gravitational settling of droplets in the upper layer of the fog body can collect some droplets and cause the formation of bigger droplets and the increase of L in the surface and adjacent layer. The dependence of L on the fog thickness (H) is quantified by a theoretical expression derived by Zhou and Ferrier (2008) for a

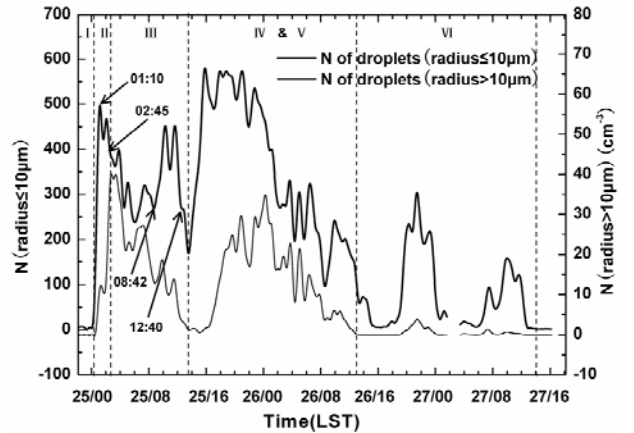


Fig. 15. The temporal evolutions of small droplet (radius $\leq 10 \mu\text{m}$) and big droplet (radius $> 10 \mu\text{m}$) number concentrations in this fog event.

steady-state fog: $L \sim H^{1/2}$. Although this expression was derived for radiation fog at the steady state and under uniform turbulence, it may also provide some hints for the estimation of L . For example, the value of L at around 0000 LST 26 December 2006 calculated using this expression is 0.6 g kg^{-1} , very close to the observed value (see Appendix C for details).

It is worth mentioning that high values of L have also been reported in fogs observed in other locations around the world. Gultepe et al. (2009) conducted three field campaigns of the Fog Remote Sensing and Modeling (FRAM) project over the following two regions of Canada: (1) the Center for Atmospheric Research Experiments (CARE) near Egbert, Ontario (FRAM-C); and (2) Lunenburg, Nova Scotia (FRAM-L). FRAM-C took place during the period from November 2005 to April 2006, and FRAM-L1 and L2 occurred during June 2006 and June 2007, respectively. In Fig. 6c of Gultepe et al. (2009), a value of $L > 0.5 \text{ g m}^{-3}$ is shown. During 2000 and 2001/2002, a campaign was carried out in Waldstein, Germany in which aspects of the physics and chemistry of fog were measured. Using the same FM-100 spectrometer, it was found that many 5-min-average values exceeded 0.5 g m^{-3} (Wrzesinsky, 2003), also shown in Fig. 2 and Table 1 of Klemm et al. (2005). Herckes et al. (2007) conducted an intensive observation in California's San Joaquin Valley during 2000/2001, in which a Gerber Scientific Particulate Volume Monitor (PVM-100) was employed to measure L . Their Fig. 1 shows that, even in a very thin fog, high L was detected with some values over 0.5 g m^{-3} . The authors found that at times the drops became so large that the fog began to form what appeared to be drizzle, similar to the results described in the current work.

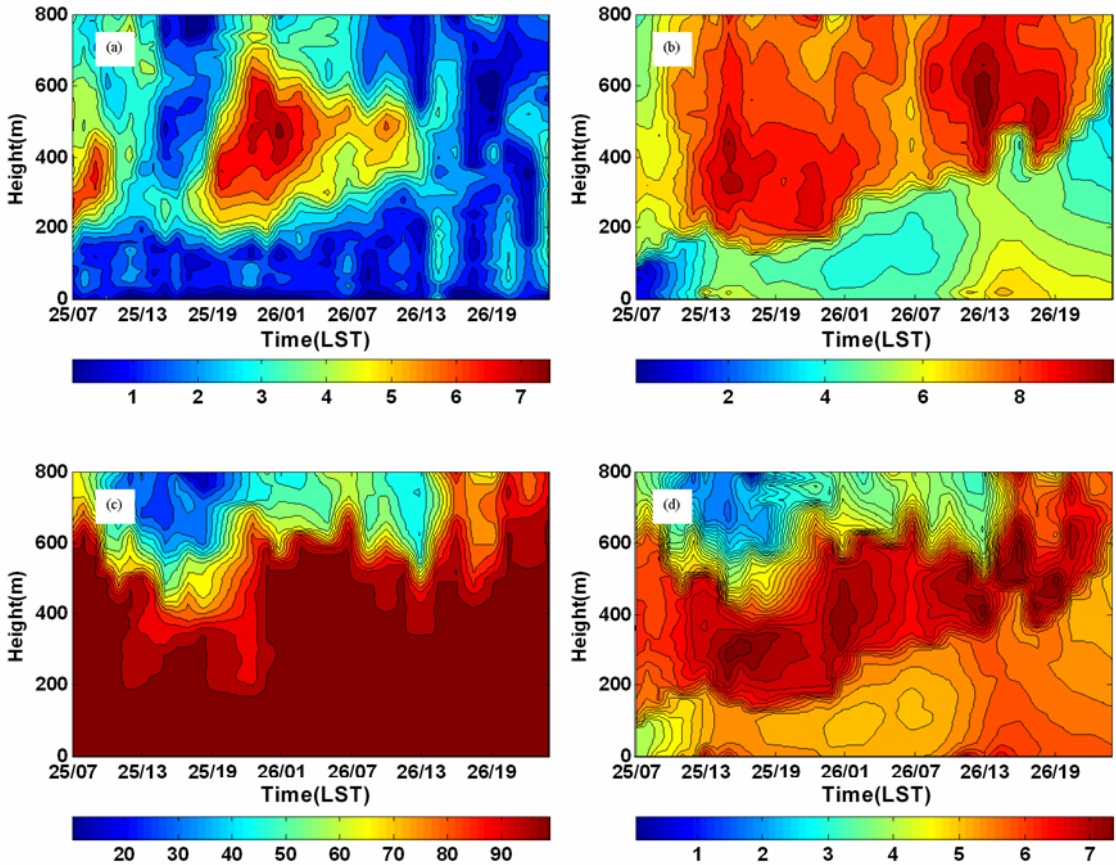


Fig. 16. Height–time cross sections of (a) wind speed (m s^{-1}), (b) temperature ($^{\circ}\text{C}$), (c) relative humidity (%), and (d) specific humidity (g kg^{-1}) during the fog event.

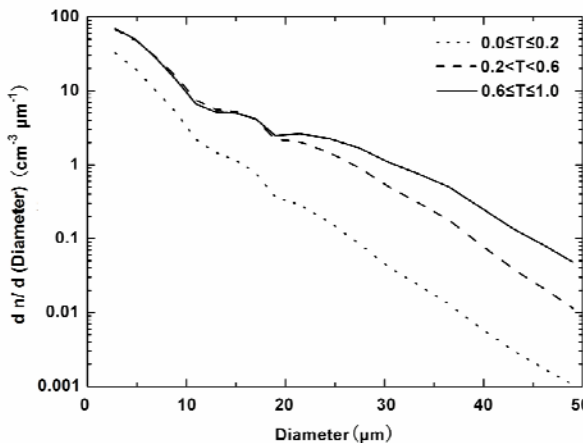


Fig. 17. Average spectra with different threshold function (T) ranges.

As discussed above, L and N show a good positive correlation. During the fog event, especially the two nights of the development stage, L and N are high. The concurrent high values of L and N conspire to cause low visibility because visibility is inversely pro-

portional to the product of L and N (Gultepe and Milbrandt, 2007).

4. Concluding remarks

An unusual fog event which occurred during the period 24–27 December 2006, and had a low visibility of $< 50 \text{ m}$ (sometimes only several meters) lasting for approximately 40 h, was encountered and observed during a field campaign conducted during the winter of that year. The measurements included fog droplet size distributions, visibility, common meteorological variables, and planetary boundary layer structure. This paper has focused on the major microphysical properties of this fog event, as well as their mutual relationships. The fog droplet size distributions have also been examined.

It was found that throughout this whole fog event, fog droplet concentration, liquid water content, mean radius and standard deviation were positively correlated to one another in general. Further analysis revealed that the positive correlations likely arose from

the dominance of droplet activation with subsequent condensational growth during the fog event. It was also found that the collection (collision and coalescence) process occurred with different degrees in different stages/periods. A stronger collection process was generally associated with weaker positive correlations, suggesting that the collection process tended to destroy some of the positive correlations, in agreement with theoretical expectation. The concurrent increases in droplet concentration, liquid water content, mean radius and standard deviation, together with a high fog top, and gravitational settlement, further led to high liquid water content and poor visibility. Statistical analysis also showed that the fog droplet size distributions, being 5-min or averaged during different stages/periods or the whole event, could all be described well by the Gamma distribution.

A few points are noteworthy in passing. First, this preliminary analysis has indicated that a main macrophysical reason for these unique microphysical properties is a stable boundary structure under the influence of warm advection with sufficient supplies of both moisture and fog condensation nuclei. A more detailed study of the macrophysics of this fog event is underway and will be reported in a follow-up paper. Second, the possibility of a positive \bar{r} - N correlation was previously pointed out by Hong and Huang (1965), and there have been other similar studies on clouds. For example, Hudson and Svensson (1995) analyzed the cloud microphysical properties off the southern California coast and found that \bar{r} and N showed negative correlations for most cases, but still in three cases the relationships were positive, which was caused by the cloud condensation nuclei plume. Considering that fog is an extreme cloud near the surface, both similarities and differences between clouds and fogs are expected. A comprehensive investigation of fogs and clouds together would be desirable to improve the understanding and parameterization of fog and cloud microphysics.

Acknowledgements. Funding for this work was mainly provided by the National Natural Science Foundation of China (Grant Nos. 40537034 and 40775012), the Natural Science Fund for Universities in Jiangsu Province (Grant Nos. 06KJA17021 and 08KJA170002), the Meteorology Fund of the Ministry of Science and Technology [Grant No. GYHY (QX) 2007-6-26], the Qing-Lan Project for cloud-fog-precipitation-aerosol study in Jiangsu Province and the Graduate Student Innovation Plan in the Universities of Jiangsu Province (CX09B_226Z). LIU Yangang was supported by the Atmospheric System Research (ASR) program of the US Department of Energy. Dr. Binbin Zhou at the NOAA Environmental Modeling Center

provided valuable suggestions.

APPENDIX A

Calculation of the Mach Number

The expression for calculating the Mach number is given by

$$M = \left\{ 2 \times \frac{C_v}{R} \times \left[\left(\frac{p_c}{p_s} + 1 \right)^{\frac{R}{c_p}} - 1 \right] \right\}^{0.5}, \quad (A1)$$

where C_v , c_p and R are specific heat at a constant volume, specific heat at a constant pressure, and a gas constant for dry air, respectively. In addition, p_c and p_s are the dynamic (pitot) pressure and static pressure, which can be converted from an analog to a digital value (AD_1) of Sensor #1 and an AD_2 value of Sensor #2 in the fog droplet spectrometer via

$$p_c = 2.4884 \times \frac{20 \times \frac{AD_1}{4095} - 10}{5} \quad (A2)$$

and

$$p_s = 68.9476 \times 3 \times (20 \times \frac{AD_2}{4095} - 10 - 1), \quad (A3)$$

respectively.

APPENDIX B

Autoconversion Threshold Function

According to Liu et al. (2005, 2006), all the autoconversion parameterizations that have been developed so far can be generically written as:

$$P = P_0 T, \quad (B1)$$

where P is the autoconversion rate, P_0 is the rate function describing the conversion rate after the onset of the autoconversion process, and T is the threshold function describing the threshold behavior of the autoconversion process. The size truncation function employed to quantify the effect of truncating the cloud droplet size distribution on the autoconversion rate can be used as a threshold function to represent the threshold behavior associated with the autoconversion process, providing a physical basis for the threshold function. The expression of T can be generally described by:

$$T = \frac{P}{P_0} = \left[\frac{\int_{r_c}^{\infty} r^6 n(r) dr}{\int_0^{\infty} r^6 n(r) dr} \right] \left[\frac{\int_{r_c}^{\infty} r^3 n(r) dr}{\int_0^{\infty} r^3 n(r) dr} \right], \quad (B2)$$

where r is the droplet radius, $n(r)$ is the cloud droplet size distribution, and r_c is the critical radius for autoconversion. Liu et al. (2004) derived an analytical expression for predicting r_c in the autoconversion parameterization:

$$r_c \approx 4.09 \times 10^{-4} \beta_{\text{con}}^{1/6} \frac{N^{1/6}}{L^{1/3}}, \quad (\text{B3})$$

where $\beta_{\text{con}} = 1.15 \times 10^{23}$ is an empirical coefficient.

APPENDIX C

Relationship between Fog Liquid Water Content and Thickness

According to the asymptotic analysis through a singular perturbation method by Zhou and Ferrier (2008), the vertical distribution of liquid water content (L) for steady radiation fog can be expressed by:

$$L(z, K) = \left[\frac{\beta(p, T_e) C_o H}{\alpha} \right]^{1/2} \times \left[\left(1 - \frac{z}{H} \right)^{1/2} - \frac{2}{1 + e^{z/\delta}} \right], \quad (\text{C1})$$

where α , H , z , K , p , and T_e are the gravitational settling parameter, depth of the fog bank, height, turbulent exchange coefficient, air pressure, and air temperature, respectively. $\beta(p, T_e) C_o$ is the condensation rate per unit mass due to cooling of the air. $C_o = -\partial T_e / \partial t$ (in K s^{-1}) is the total local cooling rate and the slope $\beta(p, T_e)$ can be expressed using the Clausius–Clapeyron equation:

$$\beta(p, T_e) = \frac{622 L_v e_s(T_e)}{R_v T_e^2 p}, \quad (\text{C2})$$

where L_v and R_v are the latent heat and the gas constant for vapor, respectively, and e_s is the saturation vapor pressure. The quantity δ can be thought of as a fog boundary layer, expressed as

$$\delta = \frac{K}{2 [\alpha \beta(p, T_e) C_o H]^{1/2}}. \quad (\text{C3})$$

Setting $K \rightarrow 0$ in Eq. (C1), the maximum possible value for the liquid water content of fog near the surface can be obtained as

$$L_{\text{max}} = \left[\frac{\beta(p, T_e) C_o H}{\alpha} \right]^{1/2}. \quad (\text{C4})$$

REFERENCES

- Beiderwieden, E., A. Schmidt, Y. J. Hsia, S. C. Chang, T. Wrzesinsky, and O. Klemm, 2007: Nutrient input through occult and wet deposition into a subtropical montane cloud forest. *Water, Air, and Soil Pollution*, **186**, 273–288.
- Costa, A. A., C. J. de Oliveira, J. C. P. de Oliveira, and A. J. d. C. Sampaio, 2000: Microphysical observations of warm cumulus clouds in Ceará Brazil. *Atmospheric Research*, **54**(2–3), 167–199.
- Croft, P. J., R. L. Pfost, J. M. Medlin, and G. A. Johnson, 1997: Fog forecasting for the southern region: A conceptual model approach. *Wea. Forecasting*, **12**(3), 545–556.
- Eldridge, R. G., 1966: Haze and fog aerosol distributions. *J. Atmos. Sci.*, **23**, 605–613.
- Eldridge, R. G., 1971: The relationship between visibility and liquid water content in fog. *J. Atmos. Sci.*, **28**, 1183–1186.
- Eugster, W., R. Burkard, F. Holwerda, F. N. Scatena, and L. A. Bruijnzeel, 2006: Characteristics of fog and fogwater fluxes in a Puerto Rican elfin cloud forest. *Agricultural and Forest Meteorology*, **139**, 288–306.
- Fuzzi, S., and Coauthors, 1992: The Po Valley fog experiment 1989: An overview. *Tellus*, **44B**, 448–468.
- García-García, F., U. Virafuentes, and G. Montero-Martínez, 2002: Fine-scale measurements of fog-droplet concentrations: A preliminary assessment. *Atmospheric Research*, **64**, 179–189.
- Gerber, H. E., 1981: Microstructure of a radiation fog. *J. Atmos. Sci.*, **38**, 454–458.
- Gerber, H. E., 1991: Supersaturation and droplet spectral evolution in fog. *J. Atmos. Sci.*, **48**, 2569–2588.
- Guedalia, D., and T. Bergot, 1994: Numerical forecasting of radiation fog. Part II: A comparison of model simulation with several observed fog events. *Mon. Wea. Rev.*, **122**, 1231–1246.
- Gultepe, I., and G. A. Isaac, 2004: An analysis of cloud droplet number concentration (Nd) for climate studies: Emphasis on constant Nd. *Quart J. Roy. Meteor. Soc.*, **130A**(602), 2377–2390.
- Gultepe, I., and J. A. Milbrandt, 2007: Microphysical observations and mesoscale model simulation of a warm fog case during FRAM project. *Pure Appl. Geophys.*, **164**, 1161–1178.
- Gultepe, I., G. A. Isaac, and K. Strawbridge, 2001: Variability of cloud microphysical and optical parameters obtained from aircraft and satellite remote sensing during RACE. *Inter. J. Climate*, **21**(4), 507–525.
- Gultepe, I., and Coauthors, 2007: Fog research: A review of past achievements and future perspectives. *Pure Appl. Geophys.*, **164**(6), 1121–1159.
- Gultepe, I., and Coauthors, 2009: The fog remote sensing and modeling field project. *Bull. Amer. Meteor. Soc.*, **90**(3), 341–359.
- Guo, X., and G. Zheng, 2009: Advances in weather modification from 1997 to 2007 in China. *Adv. Atmos. Sci.*, **26**(2), 240–252, doi: 10.1007/s00376-009-0240-

- 8.
- Herckes, P., H. Chang, T. Lee, and J. L. Jr. Collett, 2007: Air pollution processing by radiation fogs. *Water, Air, and Soil Pollution*, **181**, 65–75.
- Hong, Z., and M. Huang, 1965: The second maximum and other related characteristics of the Southern Mountain cloud spectra. *The Study on Microphysics of Cloud/Fog Precipitation in China*, Gu, Ed., Science Press, 18–29. (in Chinese)
- Hsieh, W. C., H. Jonsson, L.-P. Wang, G. Buzorius, R. C. Flagan, J. H. Seinfeld, and A. Nenes, 2009: On the representation of droplet coalescence and autoconversion: Evaluation using ambient cloud droplet size distributions. *J. Geophys. Res.*, **114**, D07201, doi: 10.1029/2008JD010502.
- Huang, Y., Y. Huang, Z. Li, B. Chen, J. Huang, and J. Gu, 2000: The microphysical structure and evolution of winter fog in Xishuangbanna. *Acta Meteorologica Sinica*, **58** (6), 715–725. (in Chinese)
- Hudson, J. G., 1980: Relationship between fog condensation nuclei and fog microstructure. *J. Atmos. Sci.*, **37**, 1854–1867.
- Hudson, J. G., and G. Svensson, 1995: Cloud microphysical relationships in California marine stratus. *J. Appl. Meteor.*, **34**(12), 2655–2666.
- Jaw, J.-J., 1966: Statistical theory of precipitation processes. *Tellus*, **18**, 722–729.
- Klemm, O., and T. Wrzesinsky, 2007: Fog deposition fluxes of water and ions to a mountainous site in Central Europe. *Tellus*, **59**, 705–714.
- Klemm, O., T. Wrzesinsky, and C. Scheer, 2005: Fog water flux at a canopy top: Direct measurement versus one-dimensional model. *Atmos. Environ.*, **39**, 5375–5386.
- Kunkel, B. A., 1984: Parameterization of droplet terminal velocity and extinction coefficient in fog models. *J. Appl. Meteor.*, **23**, 34–41.
- Li, Z., 2001: Study of fog in China over the past 40 years. *Acta Meteorologica Sinica*, **59**(5), 616–624. (in Chinese)
- Li, Z., L. Zhong, and X. Yu, 1992: The temporal-spatial distribution and physical structure of land fog in southwest China and the Changjiang River Basin. *Acta Geographica Sinica*, **47**(3), 242–251. (in Chinese)
- Li, Z., J. Huang, Y. Huang, Z. Yang, and Q. Wang, 1999a: Study on the physical process of winter valley fog in Xishuangbanna Region. *Acta Meteorological sinica*, **13**(4), 494–508. (in Chinese)
- Li, Z., J. Huang, Y. Zhou, and S. Zhu, 1999b: Physical structures of the five-day sustained fog around Nanjing in 1996. *Acta Meteorologica Sinica*, **57**(5), 622–631. (in Chinese)
- Liu, Y., 1992: Skewness and kurtosis of measured raindrop size distributions. *Atmos. Environ.*, **26A**, 2713–2716.
- Liu, Y., 1993: Statistical theory of the Marshall-Palmer distribution of raindrops. *Atmos. Environ.*, **27A**, 15–19.
- Liu, Y., and F. Liu, 1994: On the description of aerosol particle size distribution. *Atmospheric Research*, **31**(1–3), 187–198.
- Liu, Y., L. You, W. Yang, and F. Liu, 1995: On the size distribution of cloud droplets. *Atmospheric Research*, **35**(2–4), 201–216.
- Liu, Y., P. H. Daum, S. K. Chai, and F. Liu, 2002: Cloud parameterizations, cloud physics, and their connections: An overview. *Recent Research Developments in Geophysics*, Pandalai, Ed., Research Signpost Publisher, 119–142.
- Liu, Y., P. H. Daum, and R. L. McGraw, 2004: An analytical expression for predicting the critical radius in the autoconversion parameterization. *Geophys. Res. Lett.*, **31**, L06121, doi: 10.1029/2003GL019117.
- Liu, Y., P. H. Daum, and R. L. McGraw, 2005: Size truncation effect, threshold behavior, and a new type of autoconversion parameterization. *Geophys. Res. Lett.*, **32**, L11811, doi: 10.1029/2005GL022636.
- Liu, Y., P. H. Daum, R. L. McGraw, and M. Miller, 2006: Generalized threshold function accounting for effect of relative dispersion on threshold behavior of autoconversion process. *Geophys. Res. Lett.*, **33**, L11804, doi: 10.1029/2005GL025500.
- Lu, C., S. Niu, L. Tang, J. Lü, L. Zhao, and B. Zhu, 2010: Chemical composition of fog water in Nanjing area of China and its related fog microphysics. *Atmospheric Research*, **97**, 47–69, doi: 10.1016/j.atmosres.2010.03.007.
- Lu, C., S. Niu, J. Yang, and W. Wang, 2008: An observational study on physical mechanism and boundary layer structure of winter advection fog in Nanjing. *Journal of Nanjing Institute of Meteorology*, **31**(4), 520–529. (in Chinese)
- Niu, S., C. Lu, H. Yu, L. Zhao, and J. Lü, 2010: Fog research in China: An overview. *Adv. Atmos. Sci.*, **27**(3), 639–662, doi: 10.1007/s00376-009-8174-8.
- Pilié, R. J., E. J. Mack, W. C. Kocmond, C. W. Rogers, and W. J. Eadie, 1975: The life cycle of valley fog. Part I: Micrometeorological characteristics. *J. Appl. Meteor.*, **14**, 347–363.
- Pinnick, R. G., D. L. Hoihjelle, G. Fernandez, E. B. Stenmark, J. D. Lindberg, and G. B. Hoidale, 1978: Vertical structure in atmospheric fog and haze and its effects on visible and infrared extinction. *J. Atmos. Sci.*, **35**, 2020–2032.
- Pu, M., and S. Shen, 2001: The climatic characteristics and the main weather systems of Jiangsu fog. *Meteorological Decision-Making Service Manual of Jiangsu Province*, Pu and Shen, Eds., China Meteorological Press, 91–95. (in Chinese)
- Roach, W. T., R. Brown, S. J. Caughey, J. A. Garland, and C. J. Readings, 1976: The physics of radiation fog: I—A field study. *Quart. J. Roy. Meteor. Soc.*, **102**, 313–333.
- Tang, H., S. Fan, D. Wu, and X. Deng, 2002: Research of the Microphysical Structure and Evolution of Dense Fog over Nanling Mountain Area. *Acta Scientiarum Naturalium Universitatis Sunyatseni*, **41**(4), 92–96.

- (in Chinese)
- Tomasi, C., and F. Tampieri, 1976: Features of the proportionality coefficient in the relationship between visibility and liquid water content in haze and fog. *Atmosphere*, **14**, 61–76.
- Tong, Y., 2008: Haze phenomenon and analysis of the characteristics of its pollutants in Nanjing area. M.S. thesis, College of Applied Meteorology, Nanjing University of Information and Science, 58pp. (in Chinese)
- Twomey, S., 1977: The influence of pollution on the short-wave albedo of clouds. *J. Atmos. Sci.*, **34**(6), 1149–1152.
- Wendisch, M., and Coauthors, 1998: Drop size distribution and LWC in Po Valley Fog. *Contrib. Atmos. Phys.*, **71**, 87–100.
- Wrzesinsky, T., 2003: Direct measurement and evaluation of fog deposition of water and trace substances into a mountainous forest ecosystem. Ph. D. dissertation, Department of Biology, Chemistry and Geosciences, University of Bayreuth, 108pp. (in German)
- Zhou, B., and B. S. Ferrier, 2008: Asymptotic analysis of equilibrium in radiation fog. *Journal of Applied Meteorology and Climatology*, **47**, 1704–1722.